Journal of Physics: Condensed Matter

PAPER

Unconventional critical behaviors at the magnetic phase transition of $Co_3Sn_2S_2$ kagomé ferromagnet

To cite this article: Mohamed A Kassem *et al* 2021 *J. Phys.: Condens. Matter* **33** 015801

IOP Publishing Journal of Physics: Condensed Matter
J. Phys.: Condens. Matter **33** (2020) 015801 (11pp) https://doi.org/10.1088/1361-648X/abaf94

Unconventional critical behaviors at the magnetic phase transition of $Co_3Sn_2S_2$ kagomé ferromagnet

Mohamed A Kassem[1,2,3], Yoshikazu Tabata[1], Takeshi Waki[1] and Hiroyuki Nakamura[1]

[1] Department of Materials Science and Engineering, Kyoto University, Kyoto 606-8501, Japan,
[2] Department of Physics, Faculty of Science, Assiut University, Assiut 71516, Egypt

E-mail: makassem@aun.edu.eg

Received 28 May 2020, revised 31 July 2020
Accepted for publication 14 August 2020
Published 13 October 2020

Abstract

$Co_3Sn_2S_2$ has generated a growing interest as a rare example of the highly uniaxial anisotropic kagome´ferromagnet showing a combination of frustrated-lattice magnetism and topology. Recently, via precise measurements of the magnetization and AC susceptibility we have found a low-field anomalous magnetic phase (A-phase) with very slow spin dynamics that appears just below the Curie temperature (T_C). The A-phase hosts high-density domain bubbles after cooling through T_C as revealed in a previous *in-situ* Lorentz-TEM study. Here, we present further signatures of the anomalous magnetic transition (MT) at T_C revealed by a study of the critical behaviors of the magnetization and magnetocaloric effect using a high-quality single crystal. Analyses of numerous magnetization isotherms around T_C ($\simeq$177 K) using different approaches (the modified Arrot plot, Kouvel–Fisher method and magnetocaloric effect) result in consistent critical exponents that do not satisfy the theoretical predictions of standard second-order-MT models. Scaling analyses for the magnetization, magnetic entropy change and field-exponent of the magnetic entropy change, all consistently show low-field deviations below T_C from the universal curves. Our results reveal that the MT of $Co_3Sn_2S_2$ can not be explained as a conventional second-order type and suggest an anomalous magnetic state below T_C.

Keywords: Kagome ferromagnet, frustrated magnetism, critical behavior, magnetocaloric effect, ferromagnetic anomaly, anomalous magnetic transition

(Some figures may appear in colour only in the online journal)

1. Introduction

The yield of multi-q states in magnetic systems with competing interactions has become emerging frontier in condensed matter physics. Many topological phenomena, related to the nontrivial π Berry phase captured by electrons circulating around the integer-Chern number points, such as the multiferriocity and large anomalous Hall and Nernest effects have been observed in these systems [1–6]. A recently proposed model platform along these lines is the kagome´lattice of magnetic atoms [7]. Exotic states of topological nature such as magnetic skyrmions and Dirac fermionic states have been observed in kagome´ magnets [8–11]. One kagome´ ferromagnet that has received a lot of interest is $Co_3Sn_2S_2$. The compound exhibits interesting magnetic properties originating from its magnetism of quasi-two-dimensional nature with strong magnetic anisotropy [12–14]. Furthermore, it has attracted attention as a model magnetic Weyl semimetal with flat bands [9, 10, 15].

$Co_3Sn_2S_2$ crystalizes in the shandite miniral, $Ni_3Pb_2S_2$, structure (R-3m symmetry with Co at 9e(1/2,0,0), S at 6c (0,0, z) and Sn atoms occupy 3b(0,0,1/2) and 3a(0,0,0) sites), that has been presented in many configurations [9, 12, 16–19].

[3] Author to whom any correspondence should be addressed.

As shown in figure 1(a), it can simply be considered as parallel metallic layers of Co_3-Sn with Co atoms of magnetic moments in the *c*-axis direction are arranged on a kagome´ sublattice, figure 1(b), at a Co–Co distance of about 2.7 Å. The layers are separated by Sn–S_2 blocks with an interlayer distance of 4.4 Å.

We have previously measured the temperature-dependent static magnetization and AC susceptibility and reported interesting features using single crystal grown by a flux method [20]. The occurrence of an anomalous magnetic phase (A-phase) at fields below about 0.06 T in the vicinity of the Curie temperature, large splits between the field-cooled (FC) and zero-field-cooled (ZFC) magnetizations only in the low-field region, and extremely slow spin dynamics with relaxation times longer than 10 s have been observed. Quite recently we have studied the magnetic domain evolution in the A-phase in an *in-situ* Lorentz microscopic study [21]. The domain structure is typical for anisotropy-controlled material that strongly depends, as well as the domain wall (DW) motion, on the temperature, its change rate and process (heating or cooling) and the applied magnetic field. Inactive magnetic domains due to strong pinning in the low-temperature range, which should be attributed to the strong uniaxial anisotropy in this compound, is activated with increasing temperature, as a result of thermal depinning, or with increasing the applied field. The thermal activation of a DW motion approximately starts around the lower-temperature boundary of the A-phase, denoted as T_A in reference [20]. Interestingly, a spontaneous domain reorganization which is associated with DW creep has been observed in the A-phase even in the absence of an external field. While cooling the crystal through T_C, high-density mixture of rounded magnetic bubbles and chain-like domains in zero field and only bubbles at 0.001 T became visible just below T_C. In agreement with the results of the frequency-dependent AC susceptibility, the DWs were nearly static on a time scale of 10 s below 172 K. We attributed the occurrence of the A-phase to the formation of high-density bubble domains, possibly of non-trivial spin textures, and their spontaneous reorganization in the low-field region and below T_C [21]. Recent muon spin-rotation (μSR) results have presented the possibility of an emergent competitive in-plane antiferromagnetic (AFM) order that tune the Berry-curvature anomalous Hall conductivity in the temperature range of the A-phase [22].

One way to investigate for the nature of a magnetic ground state is to study the magnetic transition (MT) by analysis for the critical behavior and/or corresponding magnetocaloric effect (MCE) [23, 24]. Although the low-field A-phase of $Co_3Sn_2S_2$ is controversial, the MT can be studied as a standard second-order MT when viewed from higher fields, for example above the saturating field. Here, we study the critical behaviors of the magnetization and MCE using a high-quality single crystal of $Co_3Sn_2S_2$, which present further signatures of the MT at T_C. In consistence with the reported low-field anomalous magnetic state [20], critical scaling analyses of the magnetization and magnetic entropy changes show consistent deviations from the second-order MT universal curves, appear below T_C only at low magnetic fields ($\leqslant$0.1 T).

2. Experimental procedures

A single crystal of $Co_3Sn_2S_2$ used in this study was grown in a tipped glassy-carbon crucible of 1 cm inner diameter that was sealed in an evacuated quartz ampoule as in a previously described modified Bridgman method [25]. About 10 g crystal has been removed from the crucible and easily cleaved in the (001) plane into two equal parts, one of them is shown in the inset of figure 1(c). Crushed parts were investigated by powder x-ray diffraction (XRD) and the stoichiometric chemical composition was confirmed by the wave-length dispersive x-ray spectroscopy (SEM-WDX). The single crystallinity and orientations have been identified by Laue x-ray spectroscopy that revealed the flat shiny surface as the (001) plane. Both crystals used in the current study and that recently used in a Lorentz TEM study [21] were selected from the same batch. Magnetization measurements were performed using a quantum design, magnetic property measurement system. The temperature dependence of the magnetization has been measured at different fields from 0.5 to 100 mT following the same protocols that we previously used for a flux-grown crystal [20]. The magnetic entropy change and critical exponents were estimated from magnetization isotherms measured at temperatures from 90 to 200 K with a step of 2 K (reduced around T_C to 0.5 K) after zero-field cooling from room temperature and while decreasing the applied magnetic field from 5 to 0 T.

3. Results

3.1. Crystal quality and structure

The high quality of the synthesized large single crystal of $Co_3Sn_2S_2$ is seen in the cleaved shiny surface and clearly indicated in its Laue patterns (inset of figure 1(c)) showing the bulk-structure six-fold symmetry of the cleavage plane (001). Experimental powder XRD pattern of crushed parts of the synthesized crystal is shown with calculated pattern in the main panel of figure 1(c). No lines of extra phases rather than those of the shandite structure appear. Refinement of the experimental structure parameters by a Rietveld analysis results in lattice constants of $a = 5.3689(1)$ Å (intralayer Co–Co distance of 2.684 Å) and $c = 13.1786(3)$ Å (interlayer distance of 4.392 Å) and sulfur atomic position $z = 0.2146(1)$. A piece of the shown single crystal in the inset of figure 1(c) has been used for all measurements of the magnetization presented here below, the temperature dependence at different applied magnetic fields and the isothermal magnetization curves, M vs H, at different temperatures.

3.2. Temperature dependence of magnetization

The temperature dependence of magnetization measured at low fields of 0.5 and 5 mT after ZFC and FC processes is presented in figures 2(a) and (b) for fields applied along and perpendicular to the c axis, respectively. The low-field $M(T, H)$ with both H // c and $H \perp c$ shows a sudden increase at the Curie temperature T_C, which corresponds the reported FM transition [20, 26, 27]. While the observed slightly higher $T_C = 177$ K, comparted to $T_C = 174$ K ($\pm$1 K) exhibited by

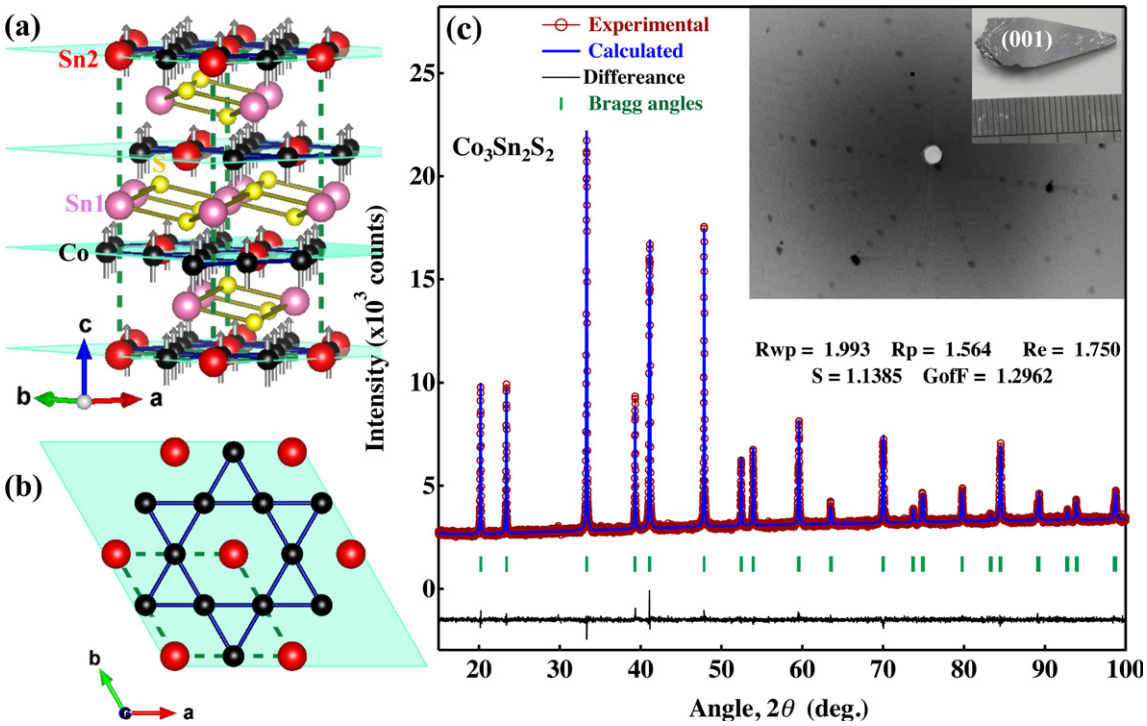

Figure 1. Structural properties and crystal quality: (a) the crystal structure of $Co_3Sn_2S_2$ showing the metallic Co_3–Sn layers separated by Sn–S_2 blocks along the *c*-axis with (b) one layer contains a Co-kagome´ sublattice projected to the (001) plane. The magnetic moments are shown along the easy *c*-axis. (c) Experimental (symbols) and Rietveld-calculated (thick solid) powder XRD patterns of crushed parts from $Co_3Sn_2S_2$ grown by a modified Birdman method (see text) and shown in the inset on a mm scale. Laue x-ray patterns on the shown cleavage plane (001) with the six-fold symmetry of the hexagon structure are presented in the inset background of (c).

flux-grown crystals [12, 18–20, 27], indicates a sample dependence [20], common features of the low-field $M(T, H)$ in the present and previous studies are found: the sudden increase of $M(T, H)$ at T_C, the large split of the ZFC and FC magnetization curves, humps in the FC-$M(T, H)$ at temperatures T_A and minima in-between T_C and T_A in the ZFC-$M(T, H)$. Other similarities are also found in the higher field $M(T, H)$ as shown in figures 2(c) and (d), namely, the anomalies are suppressed with increasing the magnetic field and disappear at and above fields compared to the saturating magnetic field, which is too high to observe when applying field in the *ab*-plane due to the high magnetic anisotropy [12, 13]. All observed anomalies indicate the reported low-field anomalous magnetic state close to T_C (A-phase) of $Co_3Sn_2S_2$.

For approaching accurate critical exponents and hence study the intrinsic scaling behaviors of the magnetization and corresponding magnetic entropy change, the influence of demagnetizing field has to be ruled out [28]. To estimate the sample-shape-dependent demagnetization factor, D, initial magnetization curves have been measured at different temperatures below T_C, as shown in the inset of figure 2(a). The initial isothermal curves at all temperatures almost exhibit identical slopes before the magnetization saturation, where a zero-internal-field condition $H_{int} = H - D\,M = 0$ is satisfied. The value of D can be estimated as the inverse of slope, $D = H_c/M_s$, where H_c and M_s are the saturating field and magnetization, respectively. A value of $D = 0.331$ is obtained for our used sample of an almost cubic shape. The magnetization and other physical quantities, such as the magnetic entropy change and its field-exponent, here below are presented as functions of H_{int}.

3.3. Critical scaling analysis of magnetization

To study the critical behavior of $Co_3Sn_2S_2$, magnetization isotherms have been measured with applying fields in the easy *c*-axis. The critical scaling analysis of magnetization is described in detail in the appendix A.

Figure 3(a) shows the isothermal magnetization as a function of the internal field, $M(H_{int}, T)$, measured at temperatures from 90 K to 200 K with a temperature interval of 2 K. The critical $M(H_{int}, T_C)$ curve at the Curie-temperature $T_C = 177$ K is shown by circles. The $M(H_{int})$ curves at $T < T_C$ show a part of square shape that becomes almost linear for $T > T_C$ which is a typical behavior for a ferromagnet.

The well-known Arrot plots, $[M(H_{int})]^2$ vs $\mu_0 H_{int}/M$, are shown in figure 3(b). The standard Arrot plot is based on the equation of state with the mean field criticality, equation (A2) in appendix A, that predicts parallel straight lines of $[M(H_{int})]^2$ vs $\mu_0 H_{int}/M$. In consistence with previous observations [12, 14], the Arrot plots of $Co_3Sn_2S_2$ exhibit linearity far above and below T_C, whereas, plots around T_C are concave curves to higher magnetization particularly in the low field region. This concaved behavior of $[M(H_{int})]^2$ vs $\mu_0 H_{int}/M$ in the vicinity of T_C indicates a non-mean-field criticality of the MT of the Co-shandite.

To approach the values of critical exponents of $Co_3Sn_2S_2$, we have first approximated the spontaneous magnetization,

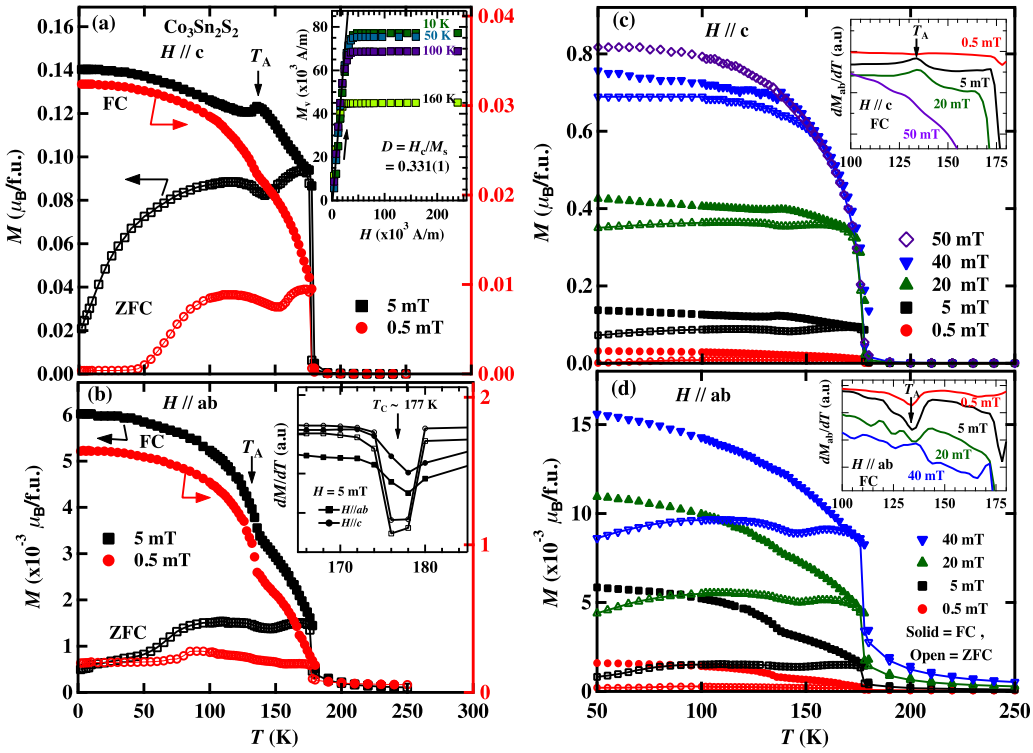

Figure 2. Temperature dependence of magnetization $M(T, H)$ of $Co_3Sn_2S_2$: $M(T, H)$ measured at different fields applied (a), (c) along and (b), (d) perpendicular to the c axis after field-cooling (closed) and zero-field cooling (open) processes and measured. Vertical arrows indicate the anomalous phase boundary, T_A. The inset of (a) shows the initial magnetization curves (volume magnetization against external field) at different temperatures and insets of (b-d) show the temperature dependence of the magnetization derivative, d$M(T, H)$/dT, at indicated fields and their directions after a FC process.

$M_s(T)$, below T_C and the initial inverse susceptibility, $\chi_0^{-1}(T)$, above T_C by extrapolating the high-field linear Arrot plot portions to $M(H_{int}) = 0$ and $\mu_0 H_{int}/M = 0$ for $T < T_C$ and $T > T_C$ data, respectively. The temperature dependences of the $M_s(T)$ and $\chi_0^{-1}(T)$ estimated from the standard Arrot plots are presented in the inset of figure 3(b). Fittings to equations (A4) and (A5) in appendix A, shown by solid lines, for $M_s(T)$ and $\chi_0^{-1}(T)$ result in critical exponents of $\beta = 0.358(9)$ and $\gamma = 1.054(24)$ as well as approximated $T_C = 178.8$ and 179.25 K, respectively. Introducing these values of β and γ to the Widom scaling relation results in $\delta = 1 + \gamma/\beta = 3.944(99)$. The inconsistently estimated critical exponents from the standard Arrot plot, namely the non-mean-field exponents estimated from the mean-field equation of state presented in table 1, indicates violation from the mean-field approximation in $Co_3Sn_2S_2$, as well as the concaved behavior of the Arrot plots does.

Hence, we have examined a further analysis using the Arrot–Noaks equation, equation (A3), with consideration of a non-mean-field criticality, i.e., the modified Arrot plot, $[M(H_{int})]^{1/\beta}$ vs $(H_{int}/M)^{1/\gamma}$. If appropriate critical exponents β and γ are adopted, the experimental data exhibits parallel straight lines and the temperature dependences of the estimated $M_s(T)$ and $\chi_0^{-1}(T)$ would be correctly described by using the adopted exponents. Practically, the values of $\beta = 0.358$ and $\gamma = 1.054$, obtained from the standard Arrot plot (figure 3(b)) have been used initially to establish a modified Arrot plot. Again, we estimated $M_s(T)$ and $\chi_0^{-1}(T)$, from the established modified Arrot plot data and obtained the critical exponents β and γ by fitting these $M_s(T)$ and $\chi_0^{-1}(T)$ to equations (A4) and (A5). The obtained exponents were used for remaking the modified Arrot plot and the procedure was iterated until parallel straight lines with unchanged critical exponents [29] have been obtained. Critical exponents and MT temperature, $\beta = 0.343(2)$, $T_C = 177.14$ K and $\gamma = 1.116(15)$, $T_C = 177.13$ K are obtained from data at $T < T_C$ and $T > T_C$, respectively. Figure 3(c) shows the modified Arrot plots $[M(H_{int})]^{1/\beta}$ vs $(H_{int}/M)^{1/\gamma}$, with the finally obtained critical exponents in this procedure. Nicely linear relation between $[M(H_{int})]^{1/\beta}$ and $(H_{int}/M)^{1/\gamma}$ is found, indicating a valid set of the critical exponents are estimated.

An alternative procedure to estimate the values of β, γ and T_C is well-known as the Kouvel–Fisher method [30]. The inset of figure 3(c) shows the linear relations of $M_S(T)\left[\mathrm{d}M_S(T)/\mathrm{d}T\right]^{-1}$ vs T and $\chi_0^{-1}(T)\left[\mathrm{d}\chi_0^{-1}(T)/\mathrm{d}T\right]^{-1}$ vs T of $Co_3Sn_2S_2$. Linear fittings to equations (A7) and (A8) result in values of $\beta = 0.338(11)$, $T_C = 177.03$ K and $\gamma = 1.137(23)$, $T_C = 176.94$ K from data at $T < T_C$ and $T > T_C$, respectively, which are close to values from direct power-function fittings to equations (A4) and (A5). Introducing the β and γ values obtained by the above two methods to the Widom relation results in $\delta = 4.254(48)$ and 4.364(129), respectively. Further, the critical exponent δ can be obtained by fitting the experimental magnetization isotherm data measured at $T \simeq T_C$ to equation (A6). The fitting results is shown by the solid line at $T = 177$ K in figure 3(a) with $\delta = 4.441(19)$,

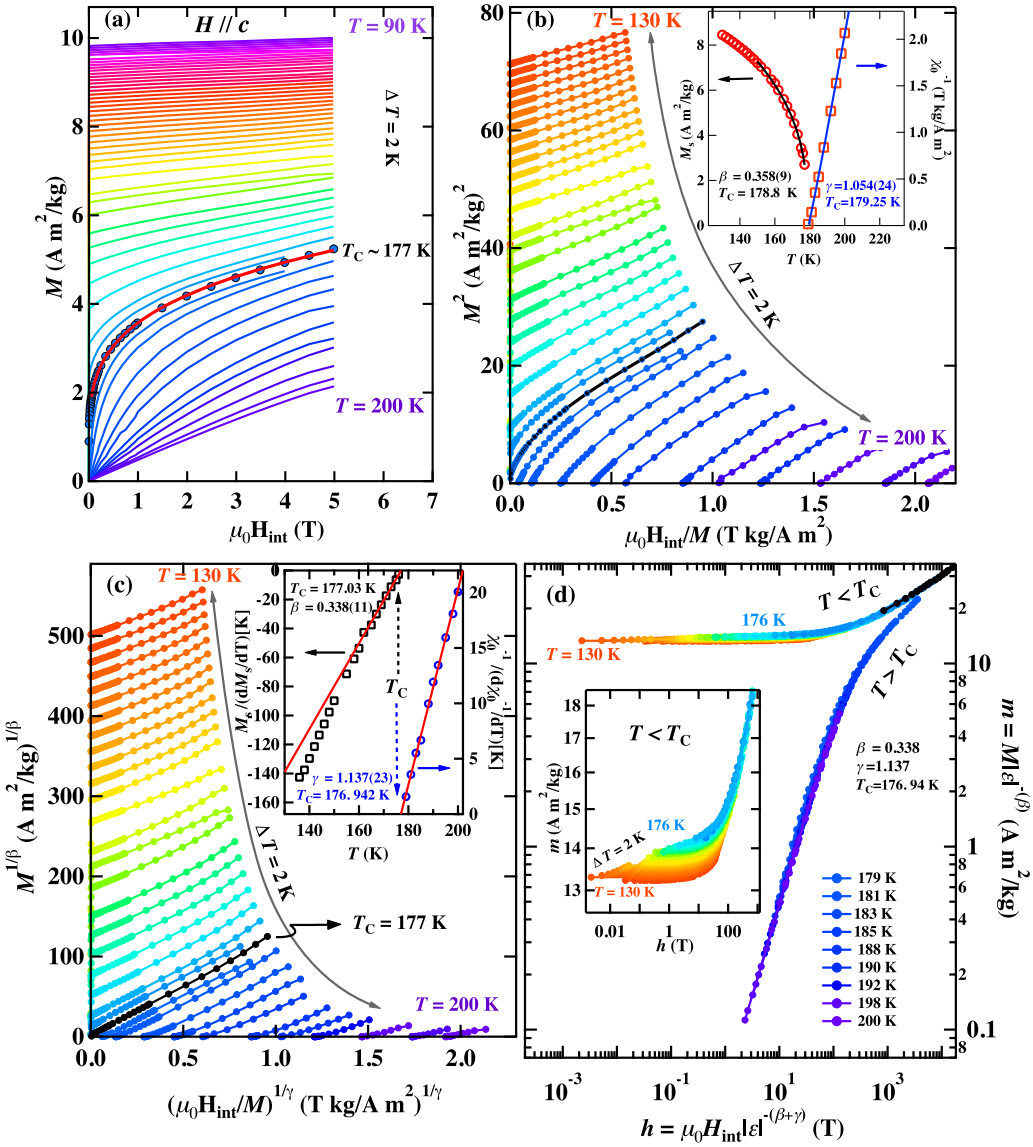

Figure 3. Critical phenomenon of $Co_3Sn_2S_2$: easy-axis magnetization isotherms measured at temperatures blow and above the shown Curie-temperature, T_C, while decreasing field from 5 T after a ZFC process, presented in the form of (a) $M(T, H)$ vs H, (b) Arrot plots, $M^2(T, H)$ vs H/M, and (c) modified Arrot plots (Arrot–Noaks form). The insets in (b) and (c) show the T-dependence of the saturated magnetization M_s and inverse susceptibility $\chi^{-1}(T, H)$ estimated by extrapolations of the Alrrot plots at $T < T_C$ and $T > T_C$, respectively, at high-fields as shown on linear scales in (b) and at the whole range of H after back and forth iterations in a Kouvel–Fisher form in the inset of (c). (d) Scaling plot of the (M–T–H) data at $T < T_C$ and $T > T_C$, based on equations (A9) and (A10) in appendix A, using the estimated critical exponents.

which is a slightly higher than the values extracted from the Arrot–Noaks plot by Widom relation, that may be due to the slight difference in the assumed T_C. The correct approximation to the critical exponents β, γ and δ is confirmed by the self-consistency among various procedures of estimation which are summarized in table 1.

An analysis of the magnetization data based on the scaling hypothesis to a universal curve for second-order MTs, described in appendix A, can help us to approximate the critical regime of $Co_3Sn_2S_2$ and may imply features of its controversial MT. Although the MT of $Co_3Sn_2S_2$ has been recently proposed as a second-order type [14], the abruptly increased magnetization at T_C and the anomalies observed in $M(T)$ below T_C with applying low magnetic fields, figure 2, all indicate a possible unconventional MT. Investigation of the critical behavior of $Co_3Sn_2S_2$ carefully performed close to the MT, i.e., at $\mu_0 H_{int} \to 0$, would be useful.

Figure 3(d) shows the scaling plot, $M(H_{int}, \varepsilon)|\varepsilon|^{-\beta}$ vs $\cdot \mu_0 H_{int}|\varepsilon|^{-(\beta+\gamma)}$, where $\varepsilon = (T - T_C)/T_C$ is the reduced temperature, for all the M–T–H_{int} data of $Co_3Sn_2S_2$ shown on a log–log scale for clarity. The scaled plot is generated based on the asymptotic equation of state in the critical regime, equations (A9) and (A3), by using the critical exponents estimated by the Kouvel–Fisher method from the modified Arrot plot. As predicted by the scaling hypothesis, it can be seen that most of the magnetization data fall onto two universal

Table 1. Comparison of critical exponents of $Co_3Sn_2S_2$ to those proposed by various models.

Experiment/Model	Method	β	γ	$\delta = 1 + \gamma/\beta$	T_C (K)[a]
	Modified Arrot plot	0.343(2)	1.116(15)	4.254(48)	177.13
$Co_3Sn_2S_2$ (this work)	Kouvel–Fisher[b]	0.338(11)	1.137(23)	4.364(129)	176.94
	Critical $M(H_{int})$[c]			4.441(19)	177
	MCE[d]	0.3928	1.3878	4.7103	177
Mean field theory	Theory	0.5	1.0	3.0	
3D Heisenberg	Theory	0.365	1.386	4.797	
3D Ising	Theory	0.325	1.241	4.818	
3D XY	Theory	0.345	1.316	4.815	
Tricritical mean-field	Theory	0.25	1.0	5.0	

[a]Estimated from data above the transition temperature.
[b]Values selected to estimate the standard critical scaling of magnetization (figure 3(d)) and MCE (figure 6).
[c]By fitting the critical magnetization isotherm $M(H, T_C)$ to equation (A6).
[d]Obtained from the MCE by fittings to equation (B4) and using relations in equation (B5).

curves, one for $T > T_C$ and another for $T < T_C$ data. However, close inspection to the $T < T_C$ data, as shown in the inset of figure 3(d), shows that the well scaled data to the universal behavior occurs only in the high fields region while the low-field data show deviations from the universal curve. The deviation in this plot occurs for the temperature-curves with $T < T_C$ down to about 140 K at crossover fields of about 0.07–0.2 T, which indicates an unconventional MT to a low-field anomalous magnetic state, as will be further discussed later below.

3.4. Critical scaling study of the magnetocaloric effect

As well as its technological interest [31], the MCE acts as an effective method to study the magnetic phase transition and even is useful to probe the nature of a magnetic ground state [24, 32–37]. The magnetic entropy change $\Delta S_M(T, H_{int}) = S(T, H_{int}) - S(T, 0)$ exhibits the critical scaling behavior [38], as well as the magnetization does, and also its sign indicates how the system is ordered by magnetic field with respect to its zero-field magnetic preferred configuration, for instance, the ferromagnetic and AFM states correspond to $\Delta S_M < 0$ and $\Delta S_M > 0$, respectively. We have studied the MCE of $Co_3Sn_2S_2$ by estimating ΔS_M based on the thermodynamic Maxwell relation after corrections for the demagnetizing field and by using the non-zero internal-field magnetization data. The derivation of ΔS_M and its critical scaling phenomena are described in appendix B.

Figure 4(a) shows the temperature dependence of $\Delta S_M(H_{int}, T)$ of $Co_3Sn_2S_2$ estimated using H_{int} and corresponding $M(H_{int}, T)$ data measured at different applied fields from 0.02 up to 5 T in a temperature range from 90 K up to 200 K. The negative values of the entropy change at all temperatures in the whole range of H corresponds to the ferromagnetically ordered ground state of $Co_3Sn_2S_2$. The peak position of ΔS_M for different field scans occurs at about 177 K where the Curie temperature T_C as the same as indicated by the critical scaling analyses of magnetization described in section 3.3.

Similar to the critical isothermal $M(H_{int}, T_C)$, the absolute value of the magnetic entropy change at T_C, $\left|\Delta S_M^{peak}(H_{int}, T_C)\right|$; the peak width of $\Delta S_M(H_{int}, T)$ around T_C, $\delta T_{FWHM}(H_{int})$; and the relative cooling power, $RCP = \left|\Delta S_M^{peak}(H_{int}, T_C)\right| \times \delta T_{FWHM}(H_{int})$, all increase with the magnetic field in power law behaviors [24], as equation (B4).

Figures 4(b)–(d) show the internal-field dependences of the estimated $|\Delta S_M(H_{int}, T)|$, δT_{FWHM} and RCP presented on log–log plots. The three quantities estimated at T_C exhibit linearity in the double-logarithmic plots, except for internal fields lower than about 0.09 T($\log(\mu_0 H_{int}) \lesssim -1$). The MCE critical exponents are estimated by fittings equation (B4) into the experimental data above 0.08 T, as $n(T_C) = 0.659$, $b = 0.5616$ and $c = 1.2123$. These MCE exponents are related with the critical exponents of magnetization as equation (B5), and thus, the critical exponents $\beta = 0.3928$, $\gamma = 1.3878$ and $\delta = 4.7103$ are obtained, which are in consistence with values estimated from the critical scaling analyses of magnetization as presented in table 1.

Following the scaling procedure described in appendix B, we have attempted the phenomenological universal scaling of the MCE [38]. We here rescale the $\Delta S_M(H_{int}, T)$ of $Co_3Sn_2S_2$ as $\left|\Delta S_M(H_{int}, T)/\Delta S_M^{peak}(H_{int}, T_C)\right|$ and plot against the reduced temperature, θ, with appropriately selecting reference temperatures $T_{r1}(H_{int})$ and $T_{r2}(H_{int})$ based on its definition in equation (B6) in appendix B. The scaling plot is shown in figure 5(a) for all $\Delta S_M(H_{int}, T)$ data measured with field scans from different fields down to zero with the reference temperatures selected at the half maximum of $\Delta S_M(H_{int}, T)$, i.e., $T_{r2}(H_{int}) - T_{r1}(H_{int}) = \delta T_{FWHM}(H_{int})$. The normalized $\Delta S_M(H_{int}, T)$ curves measured below T_C at high magnetic fields ($\mu_0 H \geqslant 0.1$ T, $\mu_0 H_{int} \gtrsim 0.08$ T) and those measured above T_C at all fields are well-scaled to a universal curve previously reported in many experimental cases [24, 34–36, 38]. However, normalized $\Delta S_M(H_{int}, T)$ curves measured at lower fields show significant deviations from the universal curve just below T_C, as seen clearly in the inset of figure 5(a). The deviations are in consistence with deviations observed in the M–T–H_{int} scaling plot in figure 3(d) and the deviations from the linear-dependences in figures 4(b)–(d), in a further indication of the unconventional MT at T_C.

As described in appendix B, the generalized temperature- and field-dependent exponent $n(H_{int}, T) = \mathrm{d}\ln\left(|\Delta S_M(H_{int}, T)|\right)/\mathrm{d}\ln(H_{int})$ also has to fall in one

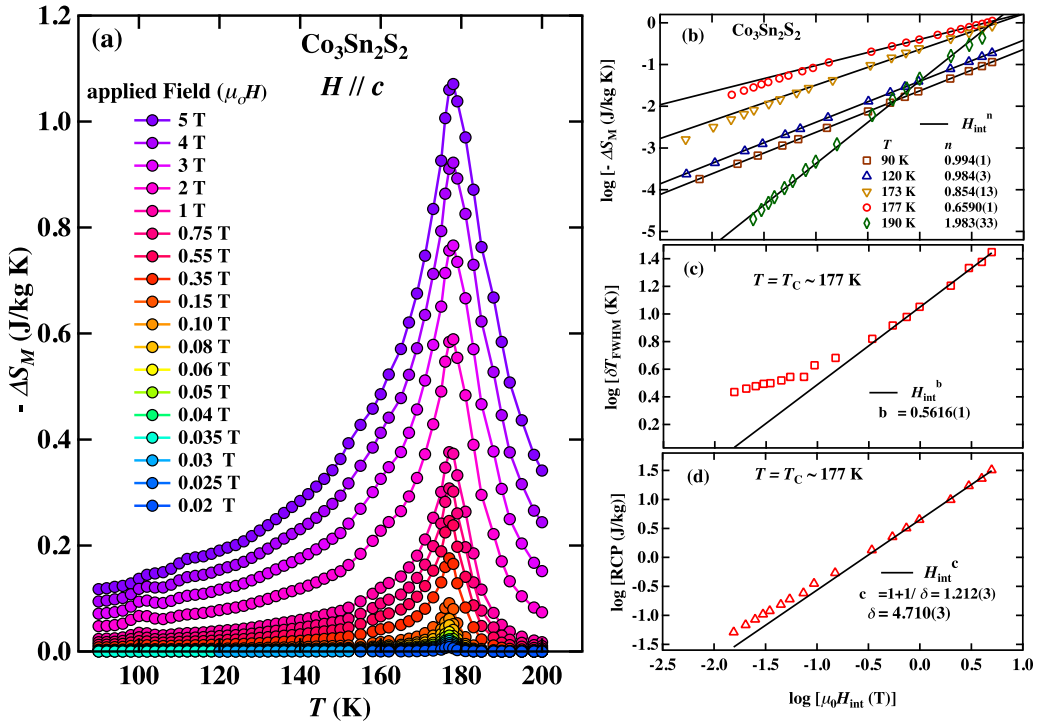

Figure 4. MCE of $Co_3Sn_2S_2$: (a) temperature dependence of the magnetic entropy change, $-\Delta S_M$, at low and high fields. The H dependence of the estimated (b) $|\Delta S_M(H_{int}, T_C)|$, (c) its peak width δT_{FWHM} (d) relative cooling power RCP $= \left|\Delta S_M^{peak}\right| \times \delta T_{FWHM}$ at indicated temperatures in log–log plots. The values of exponents n, b, c and δ are estimated by fittings to equation (B4), shown by solid lines.

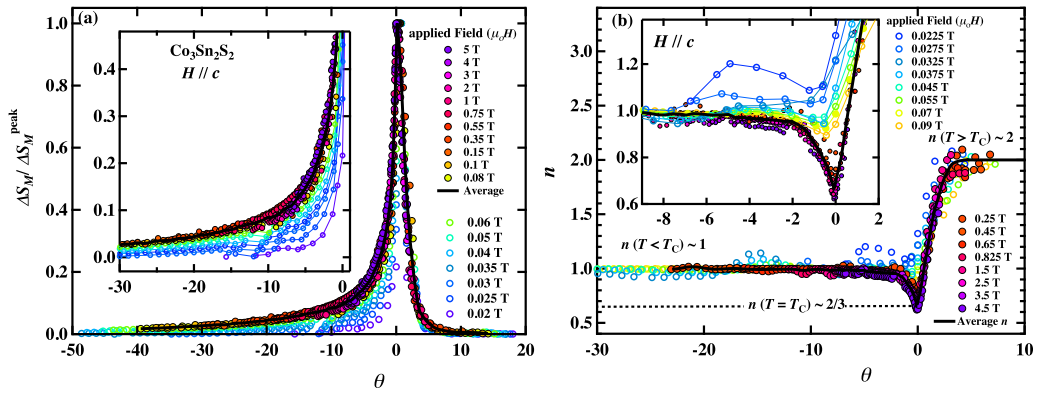

Figure 5. Phenomenological scaling of the magnetic entropy change of $Co_3Sn_2S_2$: (a) the normalized entropy change, $\Delta S_M(H,T)/\Delta S_M^{peak}(H,T)$, and (b) the generalized temperature- and field-dependent exponent $n(T,H)$, as functions of the reduced temperature, θ. Curves at low fields show significant deviations from the universal curves of second-order MTs, as shown in a magnified portion in the inset.

universal curve when plotted against the reduced temperature, θ [24, 39]. Although the demagnetizing field slightly affects ΔS_M, it has a dramatic influence on the field-exponent n [28]. We assure the estimation of $n(H_{int}, T)$ using only the equilibrium state magnetization data. Figure 5(b) shows the scaled plot of $n(H_{int}, \theta)$ for $Co_3Sn_2S_2$ using the same $T_{r1}(H_{int})$ and $T_{r2}(H_{int})$ of the scaling plot of $\left|\Delta S_M(H_{int}, T)/\Delta S_M^{peak}(H_{int}, T_C)\right|$. Similar to the scaling of $\left|\Delta S_M(H_{int}, T)/\Delta S_M^{peak}(H_{int}, T_C)\right|$, $n(H_{int}, \theta)$ correspond to fields above 0.1 T are well scaled to a universal curve in the whole temperature range, whereas the lower field $n(H_{int}, \theta)$ deviates from the universal scaling curve below T_C. As theoretically predicted for second-order MTs [24, 40], the scaled $n(H_{int}, \theta)$ at high field exhibits a minimum, $\simeq$0.65, at around T_C, $\simeq$ 177 K, and approaches 1.0 far below T_C and 2 far above T_C, which is observed here with low-field deviations only close to T_C as illustrated in figure 4(b). The values of $n(H_{int}, \theta)$, 1 and 2 far below and above T_C, respectively, are the expected value in the mean field case, and are consistent with the linear behavior far below and above T_C in the standard Arrot plot as shown in figure 3(b). We should note again that the $n(H_{int}, \theta)$ data interestingly show significant deviations from the universal curve, at and just below T_C, only at low

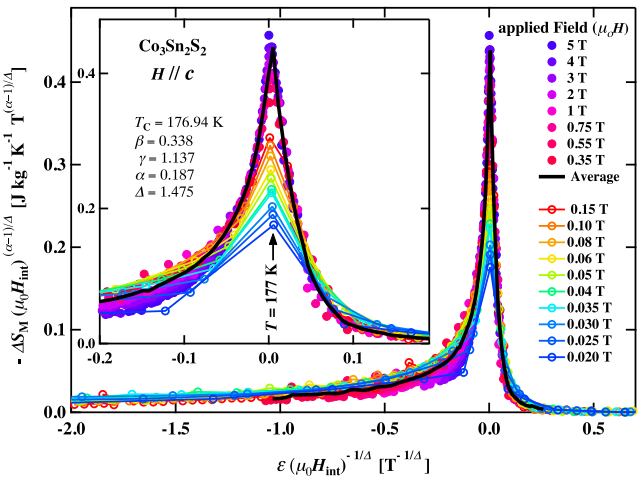

Figure 6. Standard critical scaling of the magnetic entropy changes of $Co_3Sn_2S_2$: scaling plot of the magnetic entropy change based on the equation (B7) in appendix B. The inset shows a magnification around T_C.

internal fields ($\mu_0 H_{int} < 0.08$–0.09 T at $T = 162$–177 K), which is in consistence with the scaling results of $M(H_{int}, T)$ and $\Delta S_M(H_{int}, T)$.

Finally, the standard critical scaling of $\Delta S_M(H_{int}, T)$ around the transition temperature in a system with a second order MT [24, 39], represented in equation (B7), had been attempted. Figure 6 is the scaling plot of $\Delta S_M(T, H_{int})[\mu_0 H_{int}]^{\frac{\alpha-1}{\Delta}}$ vs $\varepsilon(\mu_0 H_{int})^{-1/\Delta}$, which clearly confirms the violation of a second-order MT universality around and below T_C only at low internal fields, $\mu_0 H_{int} \lesssim 0.1$ T.

4. Discussion

In view of recent microscopic observations [21, 41], we here discuss the macroscopic features of the controversial low-filed MT to an anomalous magnetic state in the ferromagnetic phase of the anisotropic kagome ferromagnet $Co_3Sn_2S_2$ [14, 20, 21, 41, 42], based on the present critical scaling analyses of the magnetization and MCE.

Firstly, we summarize again the previously reported anomalous magnetic features observed in the macroscopic magnetization and AC susceptibility measurements [20] and their current physical interpretation based on the recent Lorentz TEM observation [21]. The abrupt increase at T_C in the static magnetization [9, 13, 20, 22], shown here in figure 2, as well as in the saturating magnetic field in the H–T phase diagram were observed [20], which are preliminary signatures of an unconventional MT at T_C. Further, the low-field anomalous magnetic state in the vicinity of T_C, named as 'A-phase', with very slow spin dynamics of relaxation time of about 10 s was found [20]. This slow-dynamics anomalous magnetic state exists only within a zero- internal-field region due to the demagnetization effect, which imply the origin of this anomalous state is domain dynamics. Indeed, characteristic spontaneous magnetic domain motion and reorganization, a spontaneous bubble domain formation, were observed by the Lorentz TEM in the temperature- and field-region of the A-phase [21] and recently via MFM investigations [41]. With slow cooling through T_C, high-density domain bubbles has been observed just below T_C only in low or zero magnetic field which should be attributed to high mobility of DWs in the A-phase [20, 21]. These observations imply us that the highly mobile domain dynamics governs the magnetic behaviors in large and long-time scales. Even in the finite internal-field region, the violation of the standard critical scaling below T_C in very low internal field is a signature of these features. In rather high field or far from T_C, the ferromagnetic spin correlations in short scale govern the magnetic behaviors and the standard ferromagnetic critical behaviors are observed, whereas, in the low field region close to T_C, the large-scaled domain dynamics become dominant and striking deviation from the standard ferromagnetic critical scaling is emergent.

Although the low magnetization of this compound that becomes lower close to T_C has limited the contrast and prevented a spin configuration inside the domain bubbles in the Lorentz TEM study [21], the relatively large bubble size excludes the skyrmions textures, at least those stabilized by the Dzaloshinski–Moriya interaction or spin frustration. Even though, skyrmionic spin textures with relatively large size have been observed in uniaxial ferromagnets which are stabilized via the classical anisotropic dipolar interaction [43]. Our currently presented results of unconventional critical behaviors with scaling break down at low fields provide a further macroscopic evidence of an anomalous MT to an expected nontrivial magnetic state in the A-phase of $Co_3Sn_2S_2$ rather than an MT to a simple FM or AFM ordered state. These observed features may be common in systems with competing interactions. Further microscopic investigations are on demand to explore the spin textures just below T_C for $Co_3Sn_2S_2$ and other uniaxial quasi-2D ferromagnets.

5. Summary

We have carefully studied the critical behaviors of the magnetization and MCE of $Co_3Sn_2S_2$ by using a high-quality single crystal. The analysis of numerous magnetization isotherms resulted in a modified Arrot plot and magnetic entropy changes around $T_C \simeq 177$ K with critical exponents ($\beta = 0.338(11)$, $\gamma = 1.137(23)$ and $\delta = 4.364(129)$) which do not satisfy predictions of the conventional theoretical models of second-order MTs. Scaling analyses of the magnetization $M(H_{int}, T)$ as well as the magnetic entropy change $\Delta S_M(H_{int}, T)$ and its field-exponent $n(H_{int}, T)$ show deviations from the universal curves in the ordered state in the vicinity of T_C only at low magnetic fields ($\mu_0 H_{int} \lesssim 0.1$ T). The deviation from the standard second-order ferromagnetic critical scaling indicate an unconventional MT to an anomalous magnetic state of $Co_3Sn_2S_2$ that needs further microscopic explorations.

Acknowledgment

MAK would like to acknowledge a fellowship the Ministry of Higher Education (Egypt) to Kyoto University, Japan.

Appendix A. Background of the critical phenomenon study

It is well known that in a second-order MT, the order parameter (i.e., magnetization M) is very small in the vicinity of the critical temperature as it changes continuously from zero. Thus, the Landau's expansion for the magnetic free energy at the ground state (that keeps a time-reversal symmetry in the absence of applied magnetic field H) and the corresponding magnetic-equilibrium equation of state with applied H are described, respectively, as [44]:

$$F_m(M) = F_m(0) + \frac{A}{2}M^2 + \frac{B}{4}M^4 + \cdots - HM, \tag{A1}$$

$$H = AM + BM^3, \tag{A2}$$

where A and B are temperature-dependent factors with B always positive while A changes its sign at the critical temperature to satisfy the zero and finite magnetizations respectively above and below the critical temperature. For a ferromagnetic system, A can have the form $A = a\varepsilon$ with $\varepsilon = (T - T_C)/T_C$ is the reduced temperature, a is a constant and T_C is the Curie temperature. Thus, equation (A2) implies a parallel line of M^2 vs H/M, the well-known Arrot plot [45], with zero abscissa and ordinate intersections for the curve at $T = T_C$.

A more general equation of the magnetic state that describes the isothermal magnetization $M(H_{int})$ around a second order MT is the Arrot–Noaks equation of state [46]:

$$\left(\frac{H}{M}\right)^{\frac{1}{\gamma}} = a\varepsilon + BM^{\frac{1}{\beta}}, \tag{A3}$$

where β and γ are two of the critical exponents and are related to a third critical exponent δ by the Widom scaling relation $\delta = 1 + \frac{\gamma}{\beta}$ [47]. The critical exponents β, γ and δ are respectively associated with the spontaneous magnetization $M_s(T) = \lim_{H\to 0} M$, the inverse initial susceptibility $\chi_0^{-1}(T) = \lim_{H\to 0}\frac{H}{M}$ and the critical magnetization isotherm $M(H, T_C)$ by the power laws [30],

$$M_S(T) = M_0(-\varepsilon)^{\beta}, \quad T < T_C(\varepsilon \text{ and } A > 0), \tag{A4}$$

$$\chi_0^{-1}(T) = \left(\frac{H}{M_0}\right)\varepsilon^{\gamma}, \quad T > T_C(\varepsilon \text{ and } A < 0) \tag{A5}$$

$$M = \Gamma H^{\frac{1}{\delta}}, \quad T = T_C(\varepsilon \text{ and } A = 0), \tag{A6}$$

where M_0, H/M_0 and Γ are the critical amplitudes of corresponding quantities. Above-mentioned equation of state (equation (A2)) is a special case with $\beta = 1/2$, $\gamma = 1$ and $\delta = 3$ (the mean-field criticality). Critical exponents of some representative models, the 3D Heisenberg, 3D Ising, 3D XY, tricritical mean-field models are listed in table 1.

Equations (A4) and (A5) can be re-formed to:

$$M_S(T)\left[\mathrm{d}M_S(T)/\mathrm{d}T\right]^{-1} = (T - T_C)\beta^{-1}, \quad \text{for } T < T_C, \tag{A7}$$

$$\chi_0^{-1}(T)\left[\mathrm{d}\chi_0^{-1}(T)/\mathrm{d}T\right]^{-1} = (T - T_C)\gamma^{-1}, \quad \text{for } T > T_C, \tag{A8}$$

Thus, the critical exponents β and γ and the MT temperature T_C can be estimated from the $M_S(T)\left[\mathrm{d}M_S(T)/\mathrm{d}T\right]^{-1}$ vs T and $\chi_0^{-1}(T)\left[\mathrm{d}\chi_0^{-1}(T)/\mathrm{d}T\right]^{-1}$ vs T plots, respectively (Kouvel–Fisher method [30]).

Based on the scaling hypothesis of the second order phase transition [48], the asymptotic equation of state in the vicinity of the MT temperature, the scaling form of the magnetization isotherms, is given as,

$$m = f_{\pm}(h), \tag{A9}$$

where

$$m = |\varepsilon|^{-\beta}M(H,\varepsilon) \quad \text{and} \quad h = H|\varepsilon|^{-(\beta+\gamma)}. \tag{A10}$$

The Arrot–Noaks equation of state, equation (A3), is a useful phenomenological expression of the scaling equation (equation (A9)). By introducing the correct values of β and γ to equation (A9), the plots of m as a function of h around T_C should fall onto two universal curves, one with the regular function f_+ for data above T_C and another with f_- for data below T_C.

In systems exhibiting an unconventional magnetic order such as chiral helimagnets [49], frustrated magnets [50] and uniaxially anisotropic van der Waals ferromagnets [51] the order parameter would be not simply the magnetization M but rather a multi-component. For instance, it can be described by a slowly varying periodic spin density in the B20 chiral helimagnets [49]. In these magnets, a metamagnetic transition drives the system from a low-field unconventional magnetic phase(s) to a field-forced ferromagnetic (FFM) state. Thus, below a critical magnetic field, these magnets usually violate the second-order MT. However, the MT thermally driven from the paramagnetic to FFM state above this critical field can be described by equation (A3) as a second-order MT with the order parameter M.

Appendix B. Magnetocaloric effect (MCE)

The change in entropy with applying magnetic field is related to the change in M with temperature by the thermodynamic Maxwell relation,

$$\left(\frac{\partial S_M(T,H)}{\partial H}\right)_T = \left(\frac{\partial M(T,H)}{\partial T}\right)_H, \tag{B1}$$

i.e., the entropy change by magnetic field $\Delta S_M(T, H) = S(T, H) - S(T, 0)$ is given by,

$$\Delta S_M(T,H) = \int_0^H \left(\frac{\partial M(T,H)}{\partial T}\right)_H \mathrm{d}H. \tag{B2}$$

In the real measurement of M isotherms at small steps of discrete fields, ΔH, and with small temperature intervals, $T_2 - T_1$, ΔS_M can be approximated as [31],

$$\Delta S_M\left(\frac{T_1+T_2}{2}, H\right) = \sum\left[\frac{M(T_2,H) - M(T_1,H)}{T_2 - T_1}\right]\Delta H. \tag{B3}$$

As the application of a magnetic field usually results in further order of the magnetic moments against thermal fluctuations, i.e., a decrease in the magnetic entropy, we observe negative ΔS_{M} in a conventional MCE. However, application of a magnetic field may result in $\Delta S_{\mathrm{M}} > 0$, that indicates a magnetic field-induced disorder with respect to the magnetic ground state, i.e., in absence of the magnetic field. Typically, the ferromagnetic and AFM ordered states correspond to the former (negative ΔS_{M}) and the latter (positive ΔS_{M}) cases, respectively.

In FM systems of second-order MT, the absolute value of the magnetic entropy change exhibits a peak at T_{C} and the peak value, $\left|\Delta S_{\mathrm{M}}^{\mathrm{peak}}(H, T_{\mathrm{C}})\right|$, usually occurs at T_{C} and increase with the applied field in power laws as [24],

$$\begin{cases} \left|\Delta S_{\mathrm{M}}^{\mathrm{peak}}(H, T_{\mathrm{C}})\right| \sim H^{n(T_{\mathrm{C}})}, \\ \delta T_{\mathrm{FWHM}}(H, T_{\mathrm{C}}) \sim H^{b}, \\ \mathrm{RCP} \sim H^{c}, \end{cases} \tag{B4}$$

The exponents $n(T_{\mathrm{C}})$, b, and c are related with the critical exponents of magnetization β, γ, and δ as,

$$\begin{cases} n(T_{\mathrm{C}}) = \dfrac{1-\alpha}{\Delta}, \\ b = \dfrac{1}{\Delta}, \\ c = n(T_{\mathrm{C}}) + b = 1 + \dfrac{1}{\delta}, \end{cases} \tag{B5}$$

where $\alpha = 2 - 2\beta - \gamma$ and $\Delta = \beta\delta = \beta + \gamma$. This relation (B5) can be obtained by substituting the differential of the Arrott–Noakes equation of state, equation (A3), $\left(\frac{\partial M(T,H)}{\partial T}\right)_H$ into equation (B2) [38, 39].

Further, a phenomenological universal scaling of the MCE was proposed [24, 39]. In this scaling procedure, the normalized magnetic entropy change $\left|\Delta S_{\mathrm{M}}(H,T)/\Delta S_{\mathrm{M}}^{\mathrm{peak}}(H, T_{\mathrm{C}})\right|$ and the temperature- and field-dependent exponent $n(H,T) = \mathrm{d}\ln\left(|\Delta S_{\mathrm{M}}(H,T)|\right)/\mathrm{d}\ln(H)$ are plotted against a reduced temperature, θ, which is obtained by imposing two reference temperatures T_{r1} and T_{r2} correspond to $\theta = \pm 1$ so that [38, 39],

$$\theta = \begin{cases} -\dfrac{T - T_{\mathrm{C}}}{T_{\mathrm{r1}} - T_{\mathrm{C}}}, & T \leqslant T_{\mathrm{C}} \\ \dfrac{T - T_{\mathrm{C}}}{T_{\mathrm{r2}} - T_{\mathrm{C}}}, & T > T_{\mathrm{C}}. \end{cases} \tag{B6}$$

In spite of lack of the theoretical foundation, this phenomenological scaling has been confirmed to successfully describe the simulation data based on the mean field criticality and many experimental data [24, 39]. Theoretically [39], a standard critical scaling form of $\Delta S_{\mathrm{M}}(H,T)$ can be derived by introducing the scaling form of $M(H,T)$, equation (A9), into equation (B2) as,

$$\Delta S_{\mathrm{M}}(T,H) = a_{\mathrm{M}}|\varepsilon|^{1-\alpha} f\left(\frac{\varepsilon}{H^{1/\Delta}}\right) = a_{\mathrm{M}} H^{\frac{1-\alpha}{\Delta}} g\left(\frac{\varepsilon}{H^{1/\Delta}}\right), \tag{B7}$$

where a_{M} is a constant and $g(x) = |x|^{1-\alpha} f(x)$. In consistence with equation (B5), this equation (B7), implies that if the magnetic entropy change is rescaled by a factor $H^{n(T_{\mathrm{C}})}$ and the reduced temperature by a factor of H^{b}, the experimental data should collapse onto the same curve [39].

ORCID iDs

Mohamed A Kassem https://orcid.org/0000-0001-8871-6078
Hiroyuki Nakamura https://orcid.org/0000-0001-7085-4800

References

[1] Leonov A O and Mostovoy M 2015 Multiply periodic states and isolated skyrmions in an anisotropic frustrated magnet *Nat. Commun.* **6** 8275
[2] Taguchi Y, Oohara Y, Yoshizawa H, Nagaosa N and Tokura Y 2001 Spin chirality, Berry phase, and anomalous Hall effect in a frustrated ferromagnet *Science* **291** 2573
[3] Diep H T (ed) 1994 *Magnetic Systems with Competing Interactions: Frustated Spin System* (Singapore: World Scientific)
[4] Tokura Y and Seki S 2010 Multiferroics with spiral spin orders *Adv. Mater.* **22** 1554
[5] Nagaosa N, Sinova J, Onoda S, MacDonald A H and Ong N P 2010 Anomalous Hall effect *Rev. Mod. Phys.* **82** 1539
[6] Hanasaki N *et al* 2008 Anomalous Nernst effects in pyrochlore molybdates with spin chirality *Phys. Rev. Lett.* **100** 106601
[7] Pereiro M, Yudin D, Chico J, Etz C, Eriksson O and Bergman A 2014 Topological excitations in a kagome magnet *Nat. Commun.* **5** 4815
[8] Hou Z *et al* 2017 Observation of various and spontaneous magnetic Skyrmionic bubbles at room temperature in a frustrated Kagome magnet with uniaxial magnetic anisotropy *Adv. Mater.* **29** 1701144
[9] Liu E *et al* 2018 Giant anomalous Hall effect in a ferromagnetic kagome-lattice semimetal *Nat. Phys.* **14** 1125
[10] Liu D F *et al* 2019 Magnetic Weyl semimetal phase in a Kagomé crystal *Science* **365** 1282–5
[11] Ye L *et al* 2018 Massive Dirac fermions in a ferromagnetic kagome metal *Nature* **555** 638
[12] Kassem M A, Tabata Y, Waki T and Nakamura H 2016 Quasi-two-dimensional magnetism in Co-based shandites *J. Phys. Soc. Japan* **85** 064706
[13] Shen J *et al* 2019 On the anisotropies of magnetization and electronic transport of magnetic Weyl semimetal $Co_3Sn_2S_2$ *Appl. Phys. Lett.* **115** 212403
[14] Yan W, Zhang X, Shi Q, Yu X, Zhang Z, Wang Q, Li S and Lei H 2018 Critical behavior of half-metallic ferromagnet Co 3 Sn 2 S 2 *Solid State Commun.* **281** 57
[15] Yin J-X *et al* 2019 Negative flat band magnetism in a spin-orbit-coupled correlated kagome magnet *Nat. Phys.* **15** 443
[16] Weihrich R, Anusca I and Zabel M 2005 Halbantiperowskite: Zur struktur der shandite M3/2AS (M = Co, Ni; A = In, Sn) und ihren typ-antitypbeziehungen *Z. Anorg. Allg. Chem.* **631** 1463–70
[17] Vaqueiro P and Sobany G G 2009 A powder neutron diffraction study of the metallic ferromagnet $Co_3Sn_2S_2$ *Solid State Sci.* **11** 513
[18] Kassem M A, Tabata Y, Waki T and Nakamura H 2015 Single crystal growth and characterization of kagomé-lattice shandites Co3Sn2−In S2 *J. Cryst. Growth* **426** 208
[19] Kassem M A, Tabata Y, Waki T and Nakamura H 2016 Structure and magnetic properties of flux grown single crystals of Co3−Fe Sn2S2 shandites *J. Solid State Chem.* **233** 8

[20] Kassem M A, Tabata Y, Waki T and Nakamura H 2017 Low-field anomalous magnetic phase in the kagome-lattice shandite $Co_3Sn_2S_2$ *Phys. Rev.* B **96** 014429
[21] Sugawara A, Akashi T, Kassem M A, Tabata Y, Waki T and Nakamura H 2019 Magnetic domain structure within half-metallic ferromagnetic kagome compound C o3 S n2 S2 *Phys. Rev. Mater.* **3** 104421
[22] Guguchia Z *et al* 2020 Tunable anomalous Hall conductivity through volume-wise magnetic competition in a topological kagome magnet *Nat. Commun.* **11** 559
[23] Wilson K G 1983 The renormalization group and critical phenomena *Rev. Mod. Phys.* **55** 583
[24] Franco V and Conde A 2010 Scaling laws for the magnetocaloric effect in second order phase transitions: from physics to applications for the characterization of materials *Int. J. Refrig.* **33** 465
[25] Holder M, Dedkov Y, Kade A, Rosner H, Schnelle W, Leithe-Jasper A, Weihrich R and Molodtsov S L 2009 Photoemission study of electronic structure of the half-metallic ferromagnet $Co_3Sn_2S_2$ *Phys. Rev.* B **79** 205116
[26] Schnelle W, Leithe-Jasper A, Rosner H, Schappacher F M, Pöttgen R, Pielnhofer F and Weihrich R 2013 Ferromagnetic ordering and half-metallic state of Sn2Co 3S2 with the shandite-type structure *Phys. Rev.* B **88** 144404
[27] Lin X, Bud'ko S L and Canfield P C 2012 Development of viable solutions for the synthesis of sulfur bearing single crystals *Phil. Mag.* **92** 2436
[28] Romero-Muñiz C, Ipus J J, Blázquez J S, Franco V and Conde A 2014 Influence of the demagnetizing factor on the magnetocaloric effect: critical scaling and numerical simulations *Appl. Phys. Lett.* **104** 252405
[29] Phan M H, Woods G T, Chaturvedi A, Stefanoski S, Nolas G S and Srikanth H 2008 Long-range ferromagnetism and giant magnetocaloric effect in type VIII Eu8Ga16Ge30 clathrates *Appl. Phys. Lett.* **93** 252505
[30] Kouvel J S and Fisher M E 1964 Detailed magnetic behavior of nickel near its Curie point *Phys. Rev.* **136** A1626
[31] Phan M-H and Yu S-C 2007 Review of the magnetocaloric effect in manganite materials *J. Magn. Magn. Mater.* **308** 325
[32] Phan M H, Frey N A, Angst M, de Groot J, Sales B C, Mandrus D G and Srikanth H 2010 Complex magnetic phases in *Solid State Commun.* **150** 341
[33] Lampen P, Bingham N S, Phan M H, Srikanth H, Yi H T and Cheong S W 2014 Macroscopic phase diagram and magnetocaloric study of metamagnetic transitions in the spin chain system Ca3Co2 O6 *Phys. Rev.* B **89** 144414
[34] Han H, Menzel D, Liu W, Ling L, Du H, Pi L, Zhang C, Zhang L and Zhang Y 2017 Scaling of the magnetic entropy change in skyrmion material Fe 0.5 Co 0.5 Si *Mater. Res. Bull.* **94** 500
[35] Ge M, Zhang L, Menzel D, Han H, Jin C, Zhang C, Pi L and Zhang Y 2015 Scaling investigation of the magnetic entropy change in helimagnet MnSi *J. Alloys Compd.* **649** 46
[36] Clements E M, Das R, Li L, Lampen-Kelley P J, Phan M H, Keppens V, Mandrus D and Srikanth H 2017 Critical Behavior and Macroscopic Phase Diagram of the Monoaxial Chiral Helimagnet Cr1/3NbS2 *Sci. Rep.* **7** 6545
[37] Hu W J, Du J, Li B, Zhang Q and Zhang Z D 2008 Giant magnetocaloric effect in the Ising antiferromagnet DySb *Appl. Phys. Lett.* **92** 192505
[38] Franco V, Blázquez J S and Conde A 2006 Field dependence of the magnetocaloric effect in materials with a second order phase transition: a master curve for the magnetic entropy change *Appl. Phys. Lett.* **89** 222512
[39] Franco V, Conde A, Romero-Enrique J M and Blázquez J S 2008 A universal curve for the magnetocaloric effect: an analysis based on scaling relations *J. Phys.: Condens. Matter* **20** 285207
[40] Dong Q Y, Zhang H W, Sun J R, Shen B G and Franco V 2008 A phenomenological fitting curve for the magnetocaloric effect of materials with a second-order phase transition *J. Appl. Phys.* **103** 116101
[41] Howlader S, Ramachandran R, Shama Y and Singh G 2020 Sheet, domain structure dynamics in the ferromagnetic Kagome-lattice Weyl semimetal $Co_3Sn_2S_2$ (arXiv:2002.02494) (accessed 8 March 2020)
[42] Shi Q, Zhang X, Yang E, Yan J, Yu X, Sun C, Li S and Chen Z 2018 Study of magnetocaloric effect in half-metallic ferromagnet $Co_3Sn_2S_2$ *Results Phys.* **11** 1004
[43] Yu X, Mostovoy M, Tokunaga Y, Zhang W, Kimoto K, Matsui Y, Kaneko Y, Nagaosa N and Tokura Y 2012 Magnetic stripes and skyrmions with helicity reversals *Proc. Natl Acad. Sci.* **109** 8856
[44] Landau L D 1937 On the theory of phase transitions *Zh. Eksp. Teor. Fiz.* **7** 19
[45] Arrott A 1957 Criterion for ferromagnetism from observations of magnetic isotherms *Phys. Rev.* **108** 1394
[46] Arrott A and Noakes J E 1967 Approximate equation of state for nickel near its critical temperature *Phys. Rev. Lett.* **19** 786
[47] Widom B 1965 Equation of state in the neighborhood of the critical point *J. Chem. Phys.* **43** 3898
[48] Stanley H E 1971 *Phase Transitions and Critical Phenomena* (London: Oxford University Press)
[49] Bak P and Jensen M H 1980 Theory of helical magnetic structures and phase transitions in MnSi and FeGe *J. Phys. C: Solid State Phys.* **13** L881
[50] Harris M J, Bramwell S T, Holdsworth P C W and Champion J D M 1998 Liquid-gas critical behavior in a frustrated pyrochlore ferromagnet *Phys. Rev. Lett.* **81** 4496
[51] Liu B, Zou Y, Zhou S, Zhang L, Wang Z, Li H, Qu Z and Zhang Y 2017 Critical behavior of the van der Waals bonded high T C ferromagnet Fe3GeTe2 *Sci. Rep.* **7** 6184